IOP Publishing Quantum Sci. Technol. 8 (2023) 045024 https://doi.org/10.1088/2058-9565/acf47b

Quantum Science and Technology

OPEN ACCESS

RECEIVED
21 February 2023

REVISED
12 July 2023

ACCEPTED FOR PUBLICATION
28 August 2023

PUBLISHED
15 September 2023

PAPER

Quantum-referenced spontaneous emission tomography

I I Faruque[1,*], **B M Burridge**[1,2], **M Banic**[3,5], **M Borghi**[4], **J E Sipe**[3], **J G Rarity**[1] and **J Barreto**[1]

[1] Quantum Engineering Technology Laboratories, University of Bristol, Bristol, United Kingdom
[2] Quantum Engineering Centre for Doctoral Training, Centre for Nanoscience & Quantum Information, University of Bristol, Bristol, United Kingdom
[3] Department of Physics, University of Toronto, 60 St. George Street, Toronto, Ontario M5S 1A7, Canada
[4] Dipartimento di Fisica, Università di Pavia, via Bassi 6, 27100 Pavia, Italy
[5] National Research Council of Canada, 100 Sussex Drive, Ottawa, Ontario K1A 0R6, Canada
[*] Author to whom any correspondence should be addressed.

E-mail: imad.faruque@bristol.ac.uk

Keywords: quantum tomography, photon pairs, nonlinear optics, quantum optics, single photon sources, integrated photonics

Supplementary material for this article is available online

Abstract

We present a method of tomography in which photon pairs from a device-under-test (DUT) are experimentally characterised by quantum interference with a reference photon pair source; we call this quantum-referenced spontaneous emission tomography (Q-SpET). In Q-SpET, the joint spectral phase (JSP) of photon pairs generated by a DUT can be reconstructed by combining four spectrally resolved interferograms. We demonstrate this theoretically and experimentally, characterising the JSP of a microresonator photon pair source. Our method is fully implemented on a chip, demonstrating the compactness, inherent phase stability, low complexity, and resource efficiency of this method.

1. Introduction

Photons play an essential role quantum technologies, with applications ranging from entanglement-based quantum networks [1–5], quantum metrology, sensing, imaging [6, 7], and information processing [8–10]. Both single photons and entangled photon pairs can be used to implement protocols that go beyond the capability of classical information processing. Entangled photons can be directly generated in nonlinear parametric processes, such as spontaneous four-wave mixing (SFWM) or spontaneous parametric down-conversion, while single photons can be obtained from pairs by heralding [11]. Photon pair generation obeys the energy and the momentum conservation laws, which imprints spectral and wavevector correlations. Measuring and controlling such correlations is of great importance. For example, the number of Schmidt modes quantifies the amount of time-energy entanglement in a pair [12], while in heralding applications the presence of correlations between the photons of a pair leads to the heralded photon being left in a mixed state [13].

We describe the state of photon pairs using their biphoton wave function, or joint spectral amplitude (JSA), a quantity that depends on the frequencies of the two photons. The square magnitude of the JSA—the joint spectral intensity (JSI)—can be measured directly using a frequency-resolved coincidence measurement [14]; or more rapidly and with a higher signal-to-noise ratio by using stimulated emission tomography (SET) [15, 16]. But the argument of the JSA—the joint spectral phase (JSP)—describes the phase correlation of photon pairs, meaning the full, complex JSA is necessary for a complete characterisation of the entanglement between a pair of photons. As a first approximation, one can use the JSI extracted from SET to infer an upper bound on spectral correlation or entanglement [16]. Using a phase-sensitive SET, one can extract the JSP of photon-pairs generated from a waveguide source [17]. However, it has recently been shown that the JSP of photon pairs generated by resonant sources cannot be extracted from a phase-sensitive SET as directly as the JSI [18]. Although data from SET can be processed and provide an estimate of the correct JSP if there is an analytical model of photon-pair generation, this may not be feasible for more complicated sources [19] where such models do not exist.

Recently, many phase-sensitive methods for the measurement of the JSA have been reported. A self-referenced approach based on Electro-Optic Shearing Interferometry has been demonstrated, which makes use of post-processing relying on Fourier filtering [20, 21]. Alternatively, a weak coherent state can act as a reference, the interference of which with the state of photon pairs can lead to a measurement of the complex biphoton wavefunction in both frequency [22] and time domains [23]. These methods rely on precise timing synchronisation with the reference, and require phase stability. Also, [22] may require additional reference lasers and possibly a stabilising method (e.g. lock-in amplifier) for the phase-sensitive interference to measure the JSA of SFWM photon pairs. Other approaches mitigate the experimental complexity with larger processing overheads associated with artificially constrained phase-retrieval algorithms [24], using a methodology that can be simplified under the assumption that the photons are highly correlated [25].

Here we present a technique that recovers the JSP through the use of quantum interference between the state of a device-under-test (DUT) and that of a reference waveguide source; hence we call our strategy 'quantum-referenced spontaneous emission tomography' (Q-SpET). A particular feature of our method is the exploitation of quantum interference between the states of two dissimilar sources, unlike most experiments reported in the literature where photons are generated by identical sources [4, 13, 26–32]. We choose a micro-racetrack resonator as a DUT because it is one of the most promising photon-pair sources in integrated quantum photonic technologies [2, 33, 34] and because it has a nontrivial JSP, unlike waveguide sources [18].

Q-SpET works under the conditions that the JSA of the DUT has a smaller bandwidth than that of the reference, and that any feature (such as chirp) in the spectral profile of the pump does not vary significantly across the JSA of the reference. We employ the JSA of a waveguide, which has a flat phase profile and a uniform amplitude over a significant frequency range, as our reference. This condition is often observed in silicon-on-insulator waveguide sources [18, 35, 36] and waveguide sources in other photonic platforms [21, 22]. The simulated JSAs of our waveguide and resonant source are in figure S3(A). Another important condition is the restriction to the weak pump regime [5, 37], in which to good approximation a single photon pair is generated either in the DUT or in the reference. In this paper the technique is fully implemented on a silicon photonic chip, ensuring inherent phase stability, low complexity, and minimal resource overhead. The footprint of our circuit is $\sim$1 mm $\times$ 0.8 mm.

2. Implementing spontaneous emission tomography

In our photonic chip, shown in figure 1, the pump light, in a coherent state $|\alpha\rangle$, enters from the left through a vertical grating coupler (VGC), and its power is then divided across two paths according to the splitting ratio η set by a MZI. The pump light in each channel can lead to the generation of photon pairs through SFWM in the structure that follows.

The upper channel leads to a spiral waveguide (W), and the lower channel to a micro-ring resonator (R). The quantum state describing the pump exiting the MZI (see the circled number 1 in figure 1) can be expressed as

$$|\Psi_1\rangle = |\sqrt{\eta}\alpha\rangle_W |i\sqrt{1-\eta}\alpha\rangle_R. \tag{1}$$

Using the normalised biphoton wavefunctions $\Phi_R(\nu_s, \nu_i)$ and $\Phi_W(\nu_s, \nu_i)$ to characterise the probability amplitudes for the generation of pairs in the resonator and waveguide respectively, where ν_s and ν_i are signal and idler frequencies, the normalised states associated with these generation processes are [38]

$$|\psi_{II}\rangle_k = \int \mathrm{d}\nu_s \mathrm{d}\nu_i \, \Phi_k(\nu_s, \nu_i) a_s^\dagger(\nu_s) a_i^\dagger(\nu_i) |\mathrm{vac}\rangle, \tag{2}$$

where $k = \{R, W\}$, $a_s^\dagger(\nu_s)$ and $a_i^\dagger(\nu_i)$ are creation operators for signal and idler photons, and $|\mathrm{vac}\rangle$ is the vacuum state. After the photon pair generation, which occurs either in the DUT or in the reference, or not at all, we use asymmetric MZIs to filter out the pump, resulting in a quantum state (at circled number 2 in figure 1) consisting of a superposition of the vacuum state and the two-photon state $|\Psi_2\rangle$

$$|\Psi_2\rangle = N_R(\eta)|\psi_{II}\rangle_R |\mathrm{vac}\rangle_W + N_W(\eta)|\mathrm{vac}\rangle_R |\psi_{II}\rangle_W, \tag{3}$$

where the factors N_R and N_W depend on the splitting ratio η and the brightness of the sources, and $|N_R|^2 + |N_W|^2 = 1$. The photon pairs from the resonator then propagate through a path-matching waveguide section, and a relative phase (θ) is applied in the waveguide arm using a thermo-optic phase-shifter.

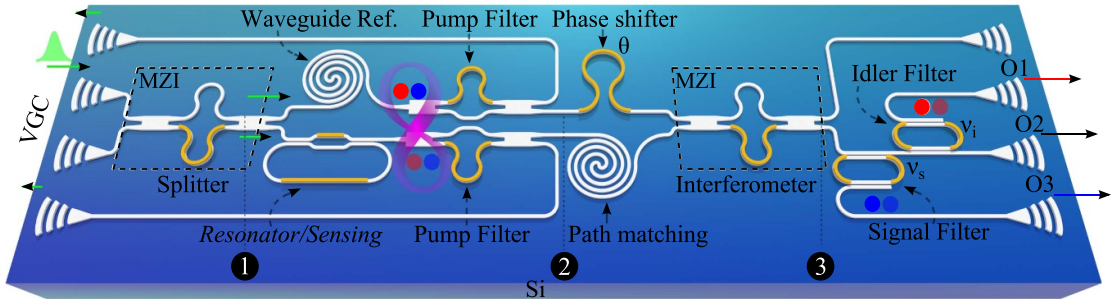

Figure 1. Schematic of our photonic chip. VGC structures are used as optical input and output (O1, O2, O3) ports. The circled numbers (1, 2, 3) refer to different stages of the circuit: First, the optical pump is distributed to the spiral and the resonator element using an MZI; the state of the pump field is described by $|\Psi_1\rangle$. In stage 2, photon pairs can be generated in either arm of the circuit, and on-chip AMZI filters are used to remove the pump from the optical channel; the two-photon state is given by $|\Psi_2\rangle$. Next, a phase θ can be applied to one of the arms using a thermal phase-shifter, before the optical path compensation (i.e. matching) element. The two arms are brought together and interfered using an Mach–Zehnder interferometer (MZI), with the resulting two-photon state given by $|\Psi_3\rangle$. Two additional tuneable on-chip optical filters based on resonator structures allow for performing frequency-resolved measurements.

Next, both arms of the circuit are connected to an MZI configured as a balanced beam splitter. After the MZI (circled number 3 in figure 1), the state describing coincidences in the lower arm of the circuit is

$$|\Psi_3\rangle = \overline{N}\int \mathrm{d}\nu_s \mathrm{d}\nu_i \left[N_R \Phi_R(\nu_s,\nu_i) - N_W \Phi_W(\nu_s,\nu_i) e^{i2\theta}\right] b_s^\dagger(\nu_s) b_i^\dagger(\nu_i)|\mathrm{vac}\rangle, \tag{4}$$

where $\overline{N}$ is a normalisation constant, and $b_j^\dagger(\nu_j)$ are creation operators for the lower output arm of the MZI. Next, we use two on-chip, resonator-based tuneable optical filters to select the frequencies of light that we divert toward a given output. Photons filtered towards O3 and O1 are labelled signal and idler, respectively, and the remaining photons propagate into O2. All three outputs are coupled off the chip using VGCs, and signal and idler photons are detected using off-chip superconducting single-photon detectors (figure S1). The probability of detecting both a signal and idler of a specific frequency in arms O3 and O1, given a phase angle θ and a splitting ratio η, involves a superposition of the amplitudes $\Phi_R(\nu_s,\nu_i)$, and $\Phi_W(\nu_s,\nu_i)$ and can be expressed as (see supplemental material):

$$P(\theta,\eta,\nu_s,\nu_i) = \frac{1}{4}\left|N_R(\eta)\Phi_R(\nu_s,\nu_i) + N_W(\eta)\Phi_W(\nu_s,\nu_i)e^{i2\theta}\right|^2. \tag{5}$$

Our method of tomography uses a chosen set of θ values ($\{0,\pi/4,3\pi/4,\pi/2\}$). At each setting of θ we sweep the on-chip filters over a range of frequencies (ν_s and ν_i) and measure the coincidences. Once normalised, these give the probability density (equation (5)) as a function of ν_s and ν_i for the value of θ chosen and the splitting ratio η of the pump. When done for the four chosen values of θ, this results in the four interferograms in figure 2(A); the resolution of our data is limited by the bandwidth of our on-chip filters (∼10 pm). Combining these results we find (see supplemental material) we can identify the JSP (denoted by θ_{JSA}) from

$$\frac{P(\frac{\pi}{4},\eta,\nu_s,\nu_i) - P(\frac{3\pi}{4},\eta,\nu_s,\nu_i)}{P(0,\eta,\nu_s,\nu_i) - P(\frac{\pi}{2},\eta,\nu_s,\nu_i)} = \frac{\mathrm{Im}\{\Phi_R(\nu_s,\nu_i)\}}{\mathrm{Re}\{\Phi_R(\nu_s,\nu_i)\}} = \tan(\theta_{\mathrm{JSA}}(\nu_s,\nu_i)), \tag{6}$$

where we have assumed that the waveguide JSA $\Phi_W(\nu_s,\nu_i)$ has negligible variation over the frequency range in which the ring JSA $\Phi_R(\nu_s,\nu_i)$ is non-negligible, and θ_{JSA} is referenced to the global phase of the waveguide JSA. Note that this strategy does not require knowledge of the precise value of the splitting ratio η of the pump.

Figure 2(B) shows both the simulated JSP, obtained following the method described earlier [39], and the JSP that we have obtained in the experiment using the results of figure 2(A). The JSPs in figure 2(B) additionally include contours (shown in white) indicating 25%, 10%, and 1% of the maximum signal intensity. These contours are extracted from the simulated JSI (figure 3(B)), and only act as a visual guide. We find good agreement between simulated and measured data, especially when the signal is above 10% of the maximum. After determining the JSP, the JSI can be identified by direct detection of the frequency dependence of the emitted signal and idler photons (figure S3(C)), or by SET [15, 18], and the full JSA can be constructed.

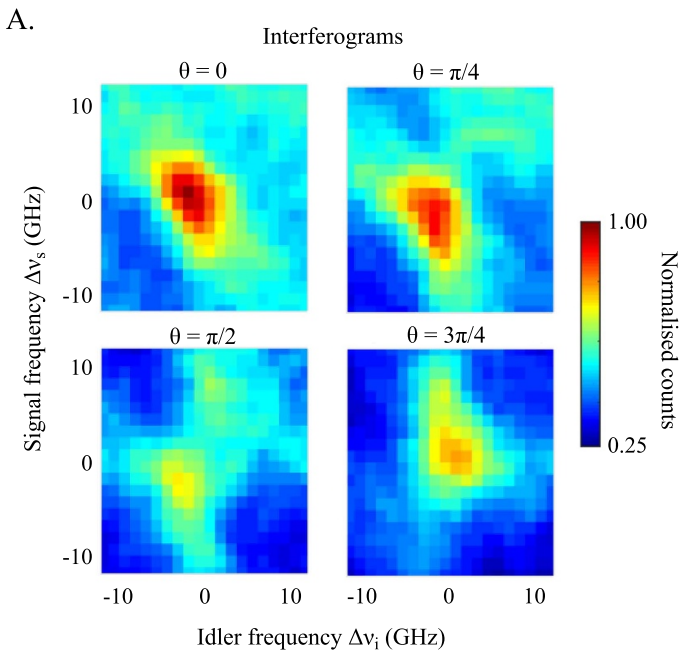

Figure 2. Spontaneous emission tomography. (A) Four measured interferograms at $\theta = \{0, \pi/4, \pi/2, 3\pi/4\}$. A low-pass filter is used here to remove high-frequency noise. (B) Simulated and experimental JSP for spontaneously emitted photon pairs generated from a micro-resonator. The superimposed white dotted contours represent constant intensity lines of the simulated JSI (figure 3(B)), indicating 25%, 10%, and 1% of the maximum signal. The colour bars are in linear scales.

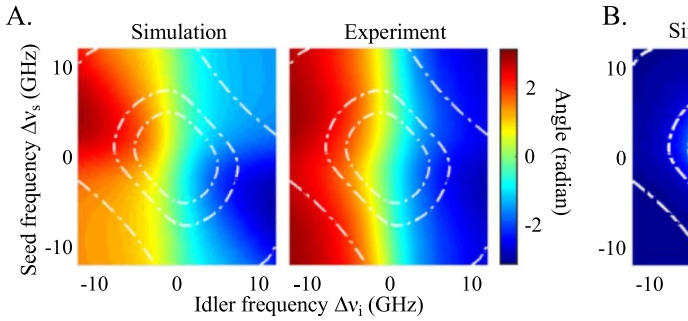

Figure 3. Stimulated emission tomography. Simulated and experimental (A) JSP and (B) JSI of the stimulated four-wave mixing in a micro-resonator. The white contour lines represent the 25%, 10%, and 1% intensity bounds as in figure 2(B)-simulation. The experimental signal is primarily detectable within the innermost contour. Considering very weak signal is present outside this contour, the experimental JSPs have remarkable similarity within the outer contours. Data was not collected in the white region in the JSI plot. The colour bars are in linear scales.

3. Stimulated vs spontaneous emission tomography of a resonant process

SET can be used to determine the JSI much more easily than direct detection of the spontaneous process. We have done SET on our integrated circuit (figures S1 and S5) using a seed at signal frequencies and recording the stimulated intensity at the idler frequencies. The results are shown in figure 3(B) together with a simulation; as in the case of Q-SpET there is reasonably good agreement between the measured and simulated data. The resolution of our SET data is 125 MHz (1 pm) and 20 MHz (0.16 pm) for the seed and idler frequencies respectively.

Just as interferograms were constructed in the Q-SpET experiment, we can construct stimulated FWM (StFWM) interferograms, here by sweeping the wavelength of an external seed laser and recording the spectra of the stimulated idler photons at O2 (see figure 1). By using the interferograms at specific values of θ, we can then extract the phase of the stimulated idler, (see supplemental material) analogously to what was done for the spontaneous process (figure 2(B)). Again, there is a reasonably good agreement between the measured data and the simulation (figure 3(A)).

Remarkably, the JSPs of the spontaneous and the stimulated processes, as can be seen when comparing figures 2 and 3, are different. For ring resonators such as the one studied here, as ν_s and ν_i are varied the

spontaneous FWM JSP (figure 2(B)) is dominated by an energy-conservation trend, angle correlation with $\Delta\nu_i$-$\Delta\nu_s$ and anti-correlation with $\Delta\nu_s$+$\Delta\nu_i$, while the JSP of the stimulated process is dominated by the value of the idler frequency $\Delta\nu_i$, with very little dependence on $\Delta\nu_s$. The difference follows from the full expressions of the JSAs for the spontaneous and stimulated processes in a ring resonator. The JSA of the SFWM process, Φ_{R-Sp}, and that for the stimulated process Φ_{R-St}, are given by

$$\Phi_{R-Sp}(\nu_s,\nu_i) = N\int \mathrm{d}\nu_{p1}\mathrm{d}\nu_{p2}\alpha(\nu_{p1})\alpha(\nu_{p2})F_{p-}(\nu_{p1})F_{p-}(\nu_{p2})F^*_{s+}(\nu_s)F^*_{i+}(\nu_i)\delta(\nu_{p1}+\nu_{p2}-\nu_s-\nu_i), \tag{7}$$

$$\Phi_{R-St}(\bar{\nu}_s,\nu_i) = N'\int \mathrm{d}\nu_{p1}\mathrm{d}\nu_{p2}\alpha(\nu_{p1})\alpha(\nu_{p2})F_{p-}(\nu_{p1})F_{p-}(\nu_{p2})F^*_{s-}(\bar{\nu}_s)F^*_{i+}(\nu_i)\delta(\nu_{p1}+\nu_{p2}-\bar{\nu}_s-\nu_i), \tag{8}$$

where the subscripts p, s, and i represent pump, signal, and idler photons respectively, and $\alpha(\nu_p)$ is the pump field amplitude. In equation (7), ν_s and ν_i are the frequencies of the spontaneously emitted signal and idler, while in equation (8), $\bar{\nu}_s$ is the CW seed frequency and ν_i is the frequency of the stimulated idler; N and N' are normalisation constants, and energy conservation is expressed by the Dirac delta function, $\delta(\nu)$. The resonant field enhancements are characterised by

$$F_{k\pm}(\nu) = \frac{1}{\sqrt{L}}\frac{\gamma^*_k}{2\pi(\nu_k-\nu)\pm i\bar{\Gamma}_k}, \tag{9}$$

where k can be pump (p), signal (s) or idler (i), γ_k is a coupling coefficient, $\bar{\Gamma}_k$ corresponds to the half-width half-maximum of the line-width of the resonances, and L is the geometrical length of the resonator [39].

Equations (7) and (8) are very similar. Indeed, the JSIs that follow from them are identical, but the JSPs are different. In particular, the resonant field enhancement factors for signal ($F^*_{s+}(\nu_s)$) in the spontaneous case and seed in the stimulated case ($F^*_{s-}(\bar{\nu}_s)$) are different, leading to different JSPs. As discussed in the supplemental material, the complex JSA for the seeded process characterising SET is proportional to the spontaneous JSA only when the seed field excites the system in one of its asymptotic-out states. For our resonator, this would require engineering the seed in such a way that the input and the loss channel of the ring are both excited, so that the seed photons can only leave the interaction region from the through port [18]. In practice, the seed can only be coupled to the input port; hence we cannot excite the resonator in one of its asymptotic-out states. The experimental conditions are then analogous to those in [18], with the direct consequence that the phase of the spontaneous JSA in equation (7) differs from the phase of the stimulated JSA in equation (8) as shown in figures 2(B) and 3(A). This confirms that, in general and without full access to all the asymptotic channels, spontaneous emission cannot be replicated by the corresponding stimulated emission process [18, 40].

4. Conclusion

In summary, Q-SpET is a resource-efficient technique that recovers the JSP of a biphoton wave function without relying on an analytical model of the photon source. It exploits the quantum interference between the biphoton wave function of a DUT and that of a dissimilar reference source. We have demonstrated this method on a silicon photonic chip by recovering the JSP of a resonator, using a waveguide source as the reference. All the components for signal splitting, photon pair generation, phase reconfiguration, and spectral filtering are integrated on the same chip, ensuring precise control and phase stability. In principle Q-SpET is not restricted to integrated photon pair sources, and could be used to characterise any biphoton quantum state; we envision this method finding applications in tasks involving the characterisation of a range of sources, and in the certification of quantum processes.

Data availability statement

The data that support the findings of this study will be openly available following an embargo at the following URL/DOI: https://doi.org/10.5523/bris.3ne98x0tsdsko2mueu5la1ysca. Data will be available from 30 September 2023.

Code availability

The MATLAB program used for processing the data is available from the corresponding author on reasonable request.

Author contributions

Authors I I F and B M B contributed equally to this work. I I F conceived the idea and method of the spontaneous emission tomography. I I F and M B designed the photonic circuit. B M B and I I F performed the experiment. B M B, I I F and J B analysed the data and performed the simulation. J E S and M B developed the analytical model. J B and J G R supervised the project. All the authors contributed to writing the manuscript.

Funding

This work was supported by the Engineering and Physical Sciences Research Council (EPSRC) under the Grant EP/L0240201. B M B acknowledges the support of the EPSRC training Grant EP/LO15730/1. The authors also acknowledge EPSRC's additional support of the work via Grants EP/M024458/1, EP/K033085/1 and EP/N015126/1. M B and J E S acknowledge support from the Natural Sciences and Engineering Research Council of Canada; M B acknowledges support from the University of Toronto Faculty of Arts & Science Top Doctoral Fellowship.

Conflict of interest

The authors declare no competing interests.

ORCID iDs

I I Faruque https://orcid.org/0000-0003-0916-2332
B M Burridge https://orcid.org/0000-0002-0950-1982

References

[1] Ekert A K 1991 Quantum cryptography based on Bell's theorem *Phys. Rev. Lett.* **67** 661–3
[2] Yin J *et al* 2017 Satellite-based entanglement distribution over 1200 kilometers *Science* **356** 1140–4
[3] Joshi S K *et al* 2020 A trusted node-free eight-user metropolitan quantum communication network *Sci. Adv.* **6** eaba0959
[4] Wang J *et al* 2018 Multidimensional quantum entanglement with large-scale integrated optics *Science* **360** 285–91
[5] Silverstone J W *et al* 2014 On-chip quantum interference between silicon photon-pair sources *Nat. Photon.* **8** 104–8
[6] Moreau P-A, Toninelli E, Gregory T and Padgett M J 2019 Imaging with quantum states of light *Nat. Rev. Phys.* **1** 367–80
[7] Barreto Lemos G B, Borish V, Cole G D, Ramelow S, Lapkiewicz R and Zeilinger A 2014 Quantum imaging with undetected photons *Nature* **512** 409–12
[8] Knill E, Laflamme R and Milburn G J 2001 A scheme for efficient quantum computation with linear optics *Nature* **409** 46–52
[9] Rudolph T 2017 Why I am optimistic about the photonic route to quantum computing *APL Photonics* **2** 030901
[10] Gentile A A, Flynn B, Knauer S, Wiebe N, Paesani S, Granade C E, Rarity J G, Santagati R and Laing A 2021 A scheme for efficient quantum computation with linear optics *Nat. Phys.* **17** 837–43
[11] Pittman T B, Jacobs B C and Franson J D 2005 Heralding single photons from pulsed parametric down-conversion *Opt. Commun.* **246** 545–50
[12] Ali-Khan I, Broadbent C J and Howell J C 2007 Large-alphabet quantum key distribution using energy-time entangled bipartite states *Phys. Rev. Lett.* **98** 060503
[13] Faruque I I, Sinclair G F, Bonneau D, Rarity J G and Thompson M G 2018 On-chip quantum interference with heralded photons from two independent micro-ring resonator sources in silicon photonics *Opt. Express* **26** 20379–95
[14] Kim Y-H and Grice W P 2005 Measurement of the spectral properties of the two-photon state generated via type II spontaneous parametric downconversion *Opt. Lett.* **30** 908–10
[15] Liscidini M and Sipe J E 2013 Stimulated emission tomography *Phys. Rev. Lett.* **111** 193602
[16] Grassani D *et al* 2016 Energy correlations of photon pairs generated by a silicon microring resonator probed by Stimulated Four Wave Mixing *Sci. Rep.* **6** 23564
[17] Jizan I, Bell B, Helt L G, Bedoya A C, Xiong C and Eggleton B J 2016 Phase-sensitive tomography of the joint spectral amplitude of photon pair sources *Opt. Lett.* **41** 4803–6
[18] Borghi M 2020 Phase-resolved joint spectra tomography of a ring resonator photon pair source using a silicon photonic chip *Opt. Express* **28** 7442–62
[19] Mittal S, Orre V V, Goldschmidt E A and Hafezi M 2021 Tunable quantum interference using a topological source of indistinguishable photon pairs *Nat. Photon.* **15** 542–8
[20] Davis A O C, Thiel V, Karpiński M and Smith B J 2018 Measuring the single-photon temporal-spectral wave function *Phys. Rev. Lett.* **121** 083602
[21] Davis A O C, Thiel V and Smith B J 2020 Measuring the quantum state of a photon pair entangled in frequency and time *Optica* **7** 1317–22
[22] Thekkadath G S, Bell B A, Patel R B, Kim M S and Walmsley I A 2022 Measuring the joint spectral mode of photon pairs using intensity interferometry *Phys. Rev. Lett.* **128** 023601
[23] Beduini F A, Zielińska J A, Lucivero V G, de Icaza Astiz Y A and Mitchell M W 2014 Interferometric measurement of the biphoton wave function *Phys. Rev. Lett.* **113** 183602
[24] MacLean J-P W, Schwarz S and Resch K J 2019 Reconstructing ultrafast energy-time-entangled two-photon pulses *Phys. Rev.* A **100** 033834

[25] Tischler N, Büse A, Helt L G, Juan M L, Piro N, Ghosh J, Steel M J and Molina-Terriza G 2015 Measurement and shaping of biphoton spectral wave functions *Phys. Rev. Lett.* **115** 193602
[26] Hong C K, Ou Z Y and Mandel L 1987 Measurement of subpicosecond time intervals between two photons by interference *Phys. Rev. Lett.* **59** 2044–6
[27] Wang X-L *et al* 2018 18-qubit entanglement with six photons' three degrees of freedom *Phys. Rev. Lett.* **120** 260502
[28] Ekert A K, Rarity J G, Tapster P R and Massimo Palma G 1992 Practical quantum cryptography based on two-photon interferometry *Phys. Rev. Lett.* **69** 1293
[29] Kok P, Lee H and Dowling J P 2002 Creation of large-photon-number path entanglement conditioned on photodetection *Phys. Rev.* A **65** 052104
[30] Fukuda H, Yamada K, Shoji T, Takahashi M, Tsuchizawa T, Watanabe T, Takahashi J-I and Itabashi S-I 2005 Four-wave mixing in silicon wire waveguides *Opt. Express* **13** 4629–37
[31] Jeffrey E, Peters N A and Kwiat P G 2004 Towards a periodic deterministic source of arbitrary single-photon states *New J. Phys.* **6** 100–100
[32] Migdall A L, Branning D and Castelletto S 2002 Tailoring single-photon and multiphoton probabilities of a single-photon on-demand source *Phys. Rev.* A **66** 053805
[33] Llewellyn D *et al* 2020 Chip-to-chip quantum teleportation and multi-photon entanglement in silicon *Nat. Phys.* **16** 148–53
[34] Zhang Y, Menotti M, Tan K, Vaidya V D, Mahler D H, Helt L G, Zatti L, Liscidini M, Morrison B and Vernon Z 2021 Squeezed light from a nanophotonic molecule *Nat. Commun.* **12** 1–6
[35] Jizan I, Helt L G, Xiong C, Collins M J, Choi D-Y, Chae C J, Liscidini M, Steel M J, Eggleton B J and Clark A S 2015 Bi-photon spectral correlation measurements from a silicon nanowire in the quantum and classical regimes *Sci. Rep.* **5** 1–9
[36] Faruque I I, Sinclair G F, Bonneau D, Ono T, Silberhorn C, Thompson M G and Rarity J G 2019 Estimating the indistinguishability of heralded single photons using second-order correlation *Phys. Rev. Appl.* **12** 054029
[37] Olislager L, Safioui J, Clemmen S, Phan Huy K P, Bogaerts W, Baets R, Emplit P and Massar S 2013 Silicon-on-insulator integrated source of polarization-entangled photons *Opt. Lett.* **38** 1960–2
[38] Yang Z, Liscidini M and Sipe J E 2008 Spontaneous parametric down-conversion in waveguides: a backward Heisenberg picture approach *Phys. Rev.* A **77** 033808
[39] Banic M, Zatti L, Liscidini M and Sipe J E 2022 Two strategies for modeling nonlinear optics in lossy integrated photonic structures *Phys. Rev.* A **106** 043707
[40] Rozema L A, Wang C, Mahler D H, Hayat A, Steinberg A M, Sipe J E and Liscidini M 2015 Characterizing an entangled-photon source with classical detectors and measurements *Optica* **2** 430–3